Earliest photic zone niches probed by ancestral microbial rhodopsins

Cathryn D. Sephus[1], Evrim Fer[2,3], Amanda K. Garcia[3], Zachary R. Adam[4,5], Edward W. Schwieterman[5,6], Betül Kaçar[3*]

1. Scripps Institution of Oceanography, University of California at San Diego, La Jolla, CA, USA
2. Microbiology Doctoral Training Program, University of Wisconsin-Madison, Madison, WI, USA
3. Department of Bacteriology, University of Wisconsin-Madison, Madison, WI, USA
4. Department of Geoscience, University of Wisconsin-Madison, Madison, WI, USA
5. Blue Marble Space Institute of Science, Seattle, WA, USA
6. Department of Earth and Planetary Sciences, University of California, Riverside, CA, USA

*To whom correspondence should be addressed: bkacar@wisc.edu

Keywords: early Earth; phototrophy; rhodopsin; radiative transfer; origins of life; biosignature; habitability

ABSTRACT

For billions of years, life has continuously adapted to dynamic physical conditions near the Earth's surface. Fossils and other preserved biosignatures in the paleontological record are the most direct evidence for reconstructing the broad historical contours of this adaptive interplay. However, biosignatures dating to Earth's earliest history are exceedingly rare. Here, we combine phylogenetic inference of primordial rhodopsin proteins with modeled spectral features of the Precambrian Earth environment to reconstruct the paleobiological history of this essential family of photoactive transmembrane proteins. Our results suggest that ancestral microbial rhodopsins likely acted as light-driven proton pumps and were spectrally tuned toward the absorption of green light, which would have enabled their hosts to occupy depths in a water column or biofilm where UV wavelengths were attenuated. Subsequent diversification of rhodopsin functions and peak absorption frequencies was enabled by the expansion of surface ecological niches induced by the accumulation of atmospheric oxygen. Inferred ancestors retain distinct associations between extant functions and peak absorption frequencies. Our findings suggest that novel information encoded by biomolecules can be used as "paleosensors" for conditions of ancient, inhabited niches of host organisms not represented elsewhere in the paleontological record. The coupling of functional diversification and spectral tuning of this taxonomically diverse protein family underscores the utility of rhodopsins as universal testbeds for inferring remotely detectable biosignatures on inhabited planetary bodies.

INTRODUCTION

Decoding the complex relationships between life and the environments it inhabits is central to reconstructing the factors that determine planetary habitability over geologic timescales. Similarly, this approach is necessary to constrain the physical limits of biological functionality, identify general principles that may govern the evolution of living systems, and aid the search for life elsewhere in our universe (Harrison 2013; McKay 2014). Planetary habitability is strongly influenced by solar insolation and photon radiance flux, which couple planetary and stellar evolution to the persistence of life (Newman 1977; Lunine 2006). Much of Earth's historical geochemical proxy record is incomplete, which imposes significant limitations on the reconstruction of planetary and solar factors that have influenced habitability and the co-evolution of life and its environments.

The information encoded in life itself may provide novel insights into how our planet has maintained planetary habitability where geologic and stellar inferences fall short. The earliest paleontological record lacks abundant, direct evidence of major metabolic and morphogenetic features (Butterfield 2007; Garcia et al. 2021), but the contemporary bioinformatic record is incredibly rich and includes several environment-sensitive biomolecular components. Reconstructing the ancestral sequences of biomolecules that are strongly coupled to habitability parameters may provide a means of extrapolating ancient biological phenotypes—and the environmental conditions that shaped them—back to the Last Universal Common Ancestor (LUCA) (Doolittle 2000; Benner 2002; Ruiz-Gonzalez and Marin 2004; Garcia 2019).

Photosensitive proteins are key intermediaries that connect intracellular chemical states, extracellular substrate availability, and solar irradiance. These biomolecules constitute a promising system for tracking ancient physical parameters that are not directly recorded in the geologic record. All known phototrophic metabolisms on Earth rely on one of three energy-converting pigments which transform light energy into chemical energy. These pigments include chlorophylls, bacteriochlorophylls, and retinal (Gómez-Conarnau 2019). Retinal-based pigment proteins, known as rhodopsins, have been found in Archaea, Bacteria, Eukarya, and giant viruses (Bryant and Frigaard 2006; Pinhassi 2016). Absolute age constraints on the oldest rhodopsins are unknown and the subject of investigation. Rhodopsin distribution across such diverse taxa has been attributed to high rates of microbial gene transfer and not necessarily evidence of rhodopsin presence in the last universal common ancestor (LUCA) (Sharma 2006). Other analyses suggest that the taxonomic distribution of rhodopsins may still be indicative of ancient origins, possibly predating the divergence of the three domains of life (Ruiz-Gonzalez and Marin 2004). Finally, it has been proposed that a primitive ion translocation functionality, perhaps comparable to that carried out by extant microbial rhodopsins, may have been present in some of the most deeply-rooted ancestors of today's microorganisms (Shalaeva 2015).

Retinal-based phototrophy utilizes a light-capture system that is simpler than its chlorophyll-based counterparts (DasSarma and Schwieterman 2018). Rhodopsin pigments are composed of one seven-transmembrane opsin protein and one retinal chromophore (Mackin 2014). Photoisomerization of the retinal chromophore within the opsin active site (also referred to as the retinal binding pocket) triggers a series of cyclical conformational changes that can directly drive ion transport across the cellular membrane, generating a proton-motive force that may be harnessed by ATP synthase to generate ATP (Racker 1974). The simple bipartite architecture

of rhodopsins has also been harnessed by biology for uses beyond ion transport, including both phototaxis and photophobia, substrate uptake, and starvation prevention (Sharma 2009; Steindler 2011; Akram 2013; Govorunova 2017). Rhodopsins can be tuned to absorb photons across much of the visible light spectrum (Engqvist et al. 2015) and have been sampled from exposed terrestrial surfaces to the sub-photic marine zone (Inoue et al. 2018). Today, microbial (type 1) rhodopsins are among the dominant energy-transducing agents that harvest solar energy in the surface ocean (Gómez-Conarnau 2019). It was suggested that the structural simplicity and functional diversity of microbial (type 1) rhodopsins may have promoted their spread to global econiches (Schwieterman et al. 2018). The combination of taxonomic distribution, phylogenetic tractability, and niche ubiquity indicates that ancestral type 1 rhodopsins are excellent candidate molecular systems for characterizing long-term conditions of habitability and paleoecology where geologic indicators are unavailable (Finkel et al. 2012; Kacar et al. 2017; Lamsdell et al. 2017).

We reconstructed the evolutionary history of microbial type 1 rhodopsins to explore ancestral properties that might serve as a guide for understanding early Earth paleoecology and habitability. Protein sequence analyses of both extant and phylogenetically inferred ancestral rhodopsins were used to constrain possible ancestral rhodopsin functions. In addition, maximum absorbance wavelength of ancestral rhodopsins was predicted by a machine-learning algorithm that models the relationship between spectral absorbance peaks and amino acid sequence (Karasuyama et al. 2018). Our analyses suggest proton-pump functionality and green wavelength absorption for the last common ancestor of ancestral type 1 rhodopsins. Green wavelength absorption is parsimonious with our modeled spectral features of the Precambrian Earth environment, providing an adaptive advantage to shallow coastal marine niches with abundant nutrients, metabolically useful light availability and attenuated phototoxic UV irradiation. The proliferation of specialized functions and the spectral tuning of rhodopsins likely resulted from the ecological upheaval wrought by the rise of atmospheric oxygen, with significant accumulation marked by the interval known as the Great Oxidation Event (GOE) approximately 2.3 billion years ago (Lyons et al. 2014; Sánchez-Baracaldo et al. 2021). The convergence of our results from reconstructed, ancestral biomolecular characteristics and indirect physical models reveals the manner by which phototrophic organisms have adapted to changing habitability parameters over billions of years.

RESULTS AND DISCUSSION

Conservation and statistical support for ancestral rhodopsin residues important for function and spectral tuning

We assembled a dataset of representative protein sequences with which to reconstruct the evolutionary history and ancestral traits of microbial rhodopsins. BLASTp (Camacho et al. 2009) was used to identify 452 homologous type 1 rhodopsin sequences from the National Center for Biotechnology Information (NCBI) non-redundant and UniProt protein databases. We additionally identified 116 homologs belonging to heliorhodopsins, a recently discovered rhodopsin class that exhibits an inverted membrane topology relative to type 1 rhodopsins and constitutes a distinct outgroup (Pushkarev 2018; Lu et al. 2019; Rozenberg et al. 2021). Animal, or type 2, rhodopsins, though exhibiting a similar seven transmembrane architecture, possess little sequence homology with microbial type 1 rhodopsins and were thus excluded from the dataset (Sharma 2006; Rozenberg et al. 2021). Our type 1 rhodopsin sequence dataset comprises four major archaeal rhodopsin groups: 1) bacteriorhodopsin, outward proton pumps; 2) halorhodopsin, inward chloride pumps; 3) sensory rhodopsin I, positive phototaxis mediators; and 4) sensory rhodopsin II, negative phototaxis mediators (Ernst 2014). The dataset also includes two major bacterial rhodopsin groups: 1) proteorhodopsin and 2) xanthorhodopsin, both outward proton pumps, with the latter distinguished by the ability to bind a second carotenoid chromophore (Ernst 2014). These taxonomically and functionally distinct lineages were resolved into their respective clades by maximum likelihood phylogenetic reconstruction (Fig. 1), producing a tree topology largely in agreement with previous analyses (Ihara 1999; Pinhassi 2016; Shibata 2018; Rozenberg et al. 2021). Alternate phylogenetic trees, generated by incorporating next-best-fit evolutionary models, reproduced this general topology (see Methods; Supplementary Fig. 1). Ancestral amino acid sequences were inferred by maximum likelihood from internal nodes of our rhodopsin phylogeny. Five of the oldest internal nodes were selected as targets for further phenotypic analysis: 1) Anc1, ancestral to bacteriorhodopsins and halorhodopsins, 2) Anc2, ancestral to sensory rhodopsins, 3) Anc3, ancestral to archaeal rhodopsins, 4) Anc4, ancestral to bacterial rhodopsins, and 5) Anc5, ancestral to all type 1 rhodopsins (Fig. 1, Supplementary Fig. 2).

Due to their deep position in the phylogenetic tree, mean site posterior probabilities for ancestors Anc1-Anc5 range between 0.55 and 0.76 (Fig. 2a; Supplementary Table 1). However,

161 statistical support is enriched for 23 ancestral binding pocket residues (<5 Å from the retinal
162 chromophore), constituting the most conserved element of microbial rhodopsin structure
163 (Kandori 2015). Mean posterior probabilities for binding pocket residues fall between 0.90 and
164 0.97 (Supplementary Table 1, 2). Nine of these residues have ≥95% mean pairwise identity
165 across all extant sequences included in our dataset (Y83, W86, P91, G122, W182, Y185, W189,
166 D212, and K216 in the bacteriorhodopsin of *Halobacterium salinarum*). Most have significant,
167 experimentally determined contributions to rhodopsin function (Greenhalgh 1993; Kusnetzow
168 1999; Babitzki 2009; Kandori 2015; Ding 2018), including the strictly conserved K216 residue
169 that is covalently bonded to retinal via a Schiff base linkage (Babitzki 2009). Other functions
170 include maintenance of the internal charge environment for ion-pumping rhodopsins (Song and
171 Gunner 2014; Kandori 2015) or mediation of transducer interactions required for phototactic
172 response in sensory rhodopsins (Sudo et al. 2006). Finally, binding pocket residues have been
173 implicated as having outsized influence in rhodopsin color tuning (Ren et al. 2001; Man 2003;
174 Inoue 2021). Thus, the enriched statistical support for ancestral binding pocket residues permits
175 sequence-based inferences of historical rhodopsin functionality.
176
177 **Ancestral type 1 rhodopsins likely acted as light-driven proton pumps**
178
179 Comparative analysis of extant variants has provided compelling circumstantial evidence that
180 primordial rhodopsins functioned as transporters (Ihara 1999), but the evolutionary progression
181 of functions or of photon absorptivity have not been explicitly demonstrated to date. As an initial,
182 global approach to constraining early rhodopsin functionality, 3D protein structures of maximum
183 likelihood ancestral sequences Anc1-Anc5 were predicted with Phyre2 (Kelley et al. 2015) and
184 used for functional annotation by the COFACTOR algorithm within the I-TASSER software
185 pipeline (Roy 2010). Modeled ancestral rhodopsin structures preserve the characteristic seven-
186 transmembrane alpha-helical fold, otherwise known as the G-protein coupled receptor fold
187 (Mackin 2014)—of extant microbial type 1 homologs (Fig. 3). Kyte and Doolittle hydropathy plots
188 for Anc1-Anc5 reveal seven highly hydrophobic regions, consistent with the conservation of
189 seven transmembrane domains (Supplementary Fig. 3). Membrane localization of ancestral
190 rhodopsins was also predicted by the SOSUI tool (Hirokawa et al. 1998) (Supplementary Table
191 3). Additionally, the ~21-residue-long C-terminal sequence of these ancestral rhodopsins form a
192 distinct hydrophilic region, indicating an orientation towards the cytoplasm as observed with
193 extant type 1 rhodopsins (Pushkarev 2018). Finally, the structure-based functional predictions
194 are consistent with early type 1 rhodopsins that carried out phototransduction, formed protein-

195 chromophore linkages, and acted as proton transmembrane transporters (Supplementary Table
196 4).
197
198 Given the comparatively high statistical support and functional significance of ancestral binding
199 pocket residues, we interrogated these specific sequence features to provide complementary
200 insights into plausible functionality of ancient rhodopsins. For extant, uncharacterized
201 rhodopsins, functional annotation is often guided by a characteristic, three-residue motif that
202 includes sites homologous to the D85, T89, and D96 residues (a.k.a., "DTD" motif) in
203 bacteriorhodopsin (*H. salinarum*) (Kandori 2015; Hasegawa et al. 2020; Inoue 2020; Rozenberg
204 et al. 2021). These sites are located within a section of the third transmembrane helix ("Helix C";
205 Fig. 3c, Fig. 4) that constitutes a portion of the retinal binding pocket. Variation in this motif is
206 strongly correlated with functional differentiation in rhodopsins. For example, "DTD" or "DTE"
207 motifs (glutamic acid replaces the D96 residue in the latter) are characteristic of
208 bacteriorhodopsins, xanthorhodopsins, and proteorhodopsins, which all function as light-driven
209 proton pumps and exhibit similar photosensitive mechanisms (Kandori 2015). By contrast,
210 chloride-pumping halorhodopsins exhibit a "TSA" motif and sensory rhodopsins instead exhibit a
211 "DTY" or "DTF" motif (Engelhard et al. 2018).
212
213 The functional correlation of the three-residue motif can be explained by the role these sites
214 play during ion binding and transfer. In proton-pumping rhodopsins, the negatively charged
215 residues of the DTD/DTE motifs are protonated during intermediate steps of the
216 bacteriorhodopsin, xanthorhodopsin, and proteorhodopsin photocycles, permitting unidirectional
217 proton transport out of the cytoplasm (Kandori 2015). By contrast, the TSA motif typical of
218 chloride-pumping rhodopsins lacks a negative charge relative to the DTD/DTE motifs, which is
219 compensated by binding of the chloride ion (Besaw et al. 2020; Inoue 2020). The functional
220 significance of these motifs has been underscored by experiments demonstrating the
221 conversion of proton-pumping bacteriorhodopsins into chloride pumps by a D85T mutation at
222 the first site of the DTD motif (Sasaki et al. 1995). In certain cases, functional predictions of
223 extant rhodopsins based on these characteristic motifs have been shown to prove reliable upon
224 experimental characterization (Hasegawa et al. 2020).
225
226 At the deepest nodes in the rhodopsin phylogeny, the most probable ancestral motifs are: 1)
227 Anc1, DTD, 2) Anc2, DTY, 3) Anc3, DTD, 4) Anc4, DTE, and 5) Anc5, DTE (Fig. 3). These
228 motifs suggest a proton-pumping function for all ancestors bearing the DTD/DTE motifs, except

229 for Anc2, which, as the common ancestor to sensory rhodopsins I and II, exhibits the DTY motif
230 consistent with extant sensory rhodopsins. Most inferred residues at these three sites have
231 posterior probabilities >0.90 for Anc1-Anc5 (Supplementary Table 2). The exceptions are in
232 Anc1, Anc3, and Anc5, for which the third site in the motif has a posterior probability of 0.71,
233 0.54, or 0.61, respectively. However, the next most likely ancestral states for these sites are
234 either aspartic acid or glutamic acid, maintaining the protonated carboxylic group observed in
235 extant proton transporters. Thus, a motif consistent with an ancestral proton-pumping function is
236 well supported for Anc1, Anc3, Anc4, and Anc5, which together suggests that other microbial
237 functions such as other forms of ion transport and phototaxis may be derived from an ancestral,
238 light-driven proton pump functionality. This model is compatible with experimental findings that
239 sensory rhodopsins, when expressed in alternate microbial hosts in the absence of associated
240 transducer proteins, retain the ability to transport protons, suggesting that the photosensory
241 function is more derived (Bogomolni et al. 1994).
242
243 The early evolution of proton transport by rhodopsins or rhodopsin-like proteins would likely
244 have provided an adaptive, simplistic means of maintaining the intracellular environment of
245 ancient cells. Life on early Earth likely faced several hurdles related to membrane permeability
246 that implicate the presence of relatively simple, membrane-spanning motive proteins proximal to
247 LUCA (Pohorille et al. 2003; Deamer and Dworkin 2005; Mulkidjanian et al. 2009). One of these
248 hurdles was circumventing the disruptive cellular tendency to expand and lyse due to the influx
249 of salts from their environment passing across their semi-permeable protocell membrane
250 (Pohorille 2009). The simplistic membrane-spanning ion-pump infrastructure of an early
251 rhodopsin could have provided cells inhabiting photic environments with the means to
252 counteract diffusive flux with a mechanism of active transport (Maloney 1985; Damer 2020).
253 Though the age of earliest proton-pumping rhodopsins is not constrained, biological preference
254 for transporting cations in lieu of anions is consistent with the proposed acidic conditions of the
255 early Archaean ocean, where a high concentration of chloride-based salts such as H^+, Na^+, K^+,
256 Ca^+, and Mg^+ would have been prevalent (Damer 2020; Ueda 2021). Acquiring a means of
257 agency over intercellular ion gradient dynamics would have permitted the maintenance of
258 transmembrane potential and chemiosmotic coupling for energy generation, a property which
259 may have been present in LUCA (Lane et al. 2010; Penny et al. 2014; Shalaeva 2015). From a
260 bioenergetic perspective, our results support the premise that a rhodopsin-like proton pump
261 could have enabled chemiosmotic coupling and simplistic energy production in primordial cells
262 (Racker 1974; Berhanu et al. 2019).

263 **The type 1 rhodopsin ancestor was likely tuned to absorb green light**
264
265 Extant rhodopsin variants exhibit absorption capacity across much of the visible spectrum. It is
266 unclear which portion of the spectrum the earliest rhodopsins would have attenuated, nor
267 whether changes in absorption would have been correlated with the diversification of new
268 functions. To understand the evolution of rhodopsin spectral tuning, we used a recently
269 developed group-LASSO-based machine-learning method (Karasuyama et al. 2018). This
270 method approximates the maximum absorbance wavelength (λ_{max}) of rhodopsin protein
271 sequences by producing a statistical model that describes the relationship between amino acids
272 within the seven transmembrane helices and absorbance features of experimentally
273 characterized homologs. The model was demonstrated to predict λ_{max} of rhodopsins with an
274 average error of ±7.8 nm. Here, λ_{max} values were predicted for extant sequences in the
275 phylogenetic dataset, inferred maximum likelihood ancestors, and alternative ancestors for
276 nodes Anc1-An5 generated to test the robustness of wavelength prediction to the statistical
277 uncertainty of ancestral sequence inference (see Methods; Fig. 2b,c)
278
279 The first-order spectral patterns predicted for ancestral rhodopsins indicate lineage- and,
280 potentially, function-specific color tuning. λ_{max} for all ancestors range between ~480 to 585 nm,
281 occupying the cyan-to-yellow range of the visible light spectrum (Fig. 1). Different rhodopsin
282 lineages, in addition to being associated with varying functions, also exhibit characteristic λ_{max}
283 values. For example, our results suggest that halorhodopsins evolved to absorb yellow light
284 (~565-585 nm) early, with secondary shifts toward green light absorption in a specific
285 sublineage. The bacteriorhodopsin, sensory rhodopsin I, and xanthorhodopsin clades largely
286 exhibit green spectral tuning (~500-565 nm), whereas shifts towards cyan (~480-500 nm)
287 absorption can be observed within the sensory rhodopsin II and proteorhodopsin clades.
288 Notable are the so-called blue-light and green-light absorbing members of the proteorhodopsin
289 clade, whose differential spectral tuning has been suggested to correlate with habitat depth of
290 host microbes in the marine environment (Ozaki et al. 2014). Because green light is attenuated
291 at shallower depths in clear water with minimal particulate matter, it has been argued that blue-
292 absorbing rhodopsins are hosted by organisms that occupy comparatively deeper portions of
293 the water column. Our λ_{max} predictions suggest that blue-light absorbing proteorhodopsins are
294 derived from a green-light absorbing ancestor. This spectral property would have been adaptive
295 for a shallow marine environment where blue light is preferentially absorbed or scattered by

suspended inorganic and organic material and the transmission of green light is favored (Mascarenhas and Keck 2018).

All oldest, maximum likelihood ancestral sequences (Anc1-Anc5) from our rhodopsin phylogeny have predicted λ_{max} values between 537 and 543 nm (Fig. 1). Anc5 is the deepest ancestral node, having both the greatest ancestral sequence uncertainty and, by extension, the greatest variation (~20 nm range) in predicted λ_{max} values across alternate ancestral reconstructions. Accounting for alternate ancestral sequence reconstructions at these same nodes, the predicted λ_{max} range for early ancestors is only expanded to ~525 to 545 nm. This range is still well within the green portion of the visible light spectrum, even if additionally accounting for the ±7.8 nm average error associated with the wavelength prediction algorithm (Karasuyama et al. 2018). Together, our spectral tuning analyses support a model wherein extant type 1 rhodopsins diversified from an ancestor tuned toward the absorption of green light.

Indicators of early rhodopsin host niche habitability and coevolution with Earth environment

Together, our results indicate that ancestral rhodopsins transported protons across the cellular membrane and exhibited spectral tuning toward green photons over a span of time encompassing Earth's early history of inhabitation. These inferences are robust both to the statistical uncertainty of our ancestral sequence reconstructions as well as the average error associated with the implemented machine-learning algorithm for predicting ancestral rhodopsin absorbance features. Despite the inherent limitations of computational analyses, our approach provides plausible constraints on early rhodopsin properties across hundreds of ancestral sequences of diverse taxonomic and functional groups. Such predictions can be further tested by the laboratory reconstruction and characterization of ancestral rhodopsins reported here.

Correlations between tuning of photon absorption and cellular function across modern variants might present a logical basis to infer the most likely niche that hosts of primordial, microbial rhodopsins would have occupied. Paleoecological and paleoenvironmental inferences based on organism-level associations and anatomical attributes are well-established in paleobiology, particularly for ecosystems that existed billions of years ago and for which sedimentological indicators are poor, absent or contested (Hofmann and Jackson 1994; Butterfield and Rainbird 1998; Adam et al. 2017). Inferences of 'phylogenetic paleoecology' based on molecule-level

330 attributes constitute a relatively new approach to these problems (Kacar et al. 2017; Lamsdell et
331 al. 2017).
332
333 Color tuning over microbial rhodopsin evolution has likely been shaped by a complex interplay
334 of both functional and environmental constraints (Man 2003; Engqvist et al. 2015; DasSarma
335 and Schwieterman 2018; Tsujimura and Ishikita 2020). Regarding the former, it is not
336 unexpected that both spectral absorbance patterns and protein function are evolutionarily
337 correlated, given the observation that many of the same rhodopsin binding pocket sites strongly
338 determine both features (Engqvist et al. 2015; Karasuyama et al. 2018; Tsujimura and Ishikita
339 2020). Our analysis likewise indicates that λ_{max} values correlate with cellular function throughout
340 rhodopsin's history. The oldest common ancestors of each clade possess comparable λ_{max}
341 values to modern counterparts, which themselves appear generally binned according to
342 functionally distinct lineages (Fig. 1).
343
344 Spectral tuning may be further segregated by the photon availability of the host environment
345 and by selective pressures to enable simultaneous optical control of distinct functions by
346 different colors of light. Host organisms containing rhodopsin variants are found almost
347 everywhere near Earth's surface, occupying a variety of different niches. For example, chloride-
348 pumping halorhodopsins are mostly limited to halophilic Archaea (Ugalde et al. 2011) and
349 maximally absorb yellow light, matching the spectral insolation peak experienced in the
350 terrestrial salt ponds in which they inhabit. By contrast, sensory rhodopsin II and
351 proteorhodopsin absorbances hosted in shallow-water photic zones are shifted towards blue
352 light, where peak spectral irradiance is attenuated by water transmissivity. Sensory rhodopsin I
353 (SRI) tuning is unique because it appears to have been shaped both by its dual roles in
354 phototactic and photophobic responses, as well as by the absorption profiles of other rhodopsin
355 proteins in the same host. In a host halobacterium, orange light activates SRI, which directs
356 flagellar motion towards the light source, but absorption of extra photons in the UV triggers
357 another cascade that stops flagella motion to avoid phototoxicity (Spudich and Bogomolni 1984;
358 Wilde and Mullineaux 2017), thereby guiding the host to wavelengths where both halorhodopsin
359 and bacteriorhodopsin absorb maximally (Sharma 2009).
360
361 Inferring the environmental constraints on early rhodopsin evolution is complicated by the fact
362 that Earth's atmospheric evolution has drastically altered the surface photon irradiance profile
363 over billions of years. Thus, we reconstructed photon irradiance profiles at various water depths

for both modern and haze-free Archean Earth scenarios, informed by an updated prescription for the composition of Earth's early atmosphere with high carbon dioxide and methane, but no oxygen (Arney 2016) (Fig. 5). These models coupled an advanced atmospheric radiative transfer model SMART (Meadows 1996) and the absorption profile of clear liquid water (Segelstein 1981). We found that the level of shielding enjoyed at the surface of Earth today in a haze-free Archean atmosphere is only possible at depths of tens of meters or deeper, and that the equivalent protective depth level is a strong function of wavelength. At visible wavelengths, red and infrared photons also become strongly attenuated with depth, leading to a wavelength of maximum transparency at ~485 nm in the blue-green portion of the visible spectrum (assuming no impurities, particulate matter will preferentially scatter blue light over green light). This contrasts with a peak spectral irradiance at Earth's surface without water attenuation, which ranges from roughly 500-530 nm with a corresponding color of cyan-green.

In addition to reconstructing historical changes in Earth surface irradiation, we explored the impact that the GOE (Lyons et al. 2014), one of the most significant environmental transitions in Earth-life coevolution, may have had in the evolutionary diversification of microbial type 1 rhodopsins. Light and oxygen both destroy the rhodopsin-associated retinal easily (Hampp and Oesterhelt 2004), so the various functions of rhodopsins as sensors of these external parameters are intimately tied to sequence changes throughout the phylogenetic family. The last common ancestor of haloarchaea is thought to have possessed the halorhodopsin (and perhaps a bacteriorhodopsin) gene (Sharma 2007). As haloarchaea are oxygen-consuming heterotrophs, they would likely have originated only after the rise of oxygenic photosynthesis (Schwieterman et al. 2018), constraining the maximum age of the halorhodopsin clade to at least the GOE at ~2.3 Ga, and perhaps as far back as the first indicators of oxygenation around 3.0 Ga (Olson et al. 2013; Cardona 2018). Furthermore, sensory rhodopsin II further drives a photophobic response under conditions of abundant oxygen to avoid photooxidative damage, a function that likely evolved after the emergence of a well oxygenated post-GOE environment. Because oxygen is typically required for the synthesis of retinal, it is possible that earliest microbial rhodopsins could only have originated following the GOE or potentially the (likely hundreds of millions of years earlier) emergence of oxygenic photosynthesis. However, it has been demonstrated that rhodopsin-based phototrophy can also be carried out in hypoxic and anoxic conditions (DasSarma et al. 2012). In addition, an alternative, uncharacterized biosynthetic pathway for retinal synthesis has been reported (Nakajima et al. 2020; Chazan et al. 2022). Thus, the necessity of oxygen for retinal synthesis remains an open question. Despite

ambiguity in the timing of rhodopsin origins relative to the GOE (Burnetti and Ratcliff 2020), it seems reasonable that the expansion of oxygenated niches following the GOE aided the ecological and functional diversification of rhodopsins, both expressed in the color tuning trends we observe in our phylogenetic analysis.

There are currently no absolute age constraints on either the oldest rhodopsin-bearing organisms or their biomolecular components, but an assessment of the distribution of light-driven sodium/proton export pumps among prokaryotes has been interpreted as indicating proximity of rhodopsin-like sodium translocation to the shared bacterial-archaeal superfamily ancestor (Shalaeva 2015). This would place the deepest proton-pumping ancestral nodes of our phylogenetic tree proximal to LUCA, with inferred ages of greater than ~3.5 Ga, potentially preceding the divergence of the three domains of life (Ruiz-Gonzalez and Marin 2004). Considering such an early rhodopsin origin as a possible evolutionary scenario, one interpretation is that the earliest green-absorbing rhodopsins would have been well adapted to the water transmission peak at blue-green wavelengths in the marine early Earth surface environment – even at moderate depths in the ocean such that their host organisms could escape damaging UV rays prior to the accumulation of protective atmospheric ozone (Fig. 5a,b, Fig. 6). These spectral regions notably occupy the window excluded by the absorption peaks of chlorophylls and bacteriochlorophylls, potentially reflecting the evolutionary tradeoffs between retinal- and chlorophyll-/bacteriochlorophyll-based phototrophy (Burnetti and Ratcliff 2020)(Fig. 5d, Fig. 6b). Rhodopsin terrestrial and surface water host niches following the GOE might then have later been expanded by reduced UV irradiance, with shallow water niches more sharply discriminated by the increase in dissolved oxygen concentrations, contributing to the extant pattern of functional and sequence divergence of the rhodopsin protein family. Such a scenario would be broadly compatible with trends in mid-to-late Precambrian microfossil abundance, which (questions of taphonomic bias aside) consistently indicate significant microfossil diversity and abundance in near-shore marine deposits (Adam 2016; Javaux 2017). Host microorganisms residing in these photic zones would have been able to access available nutrients (e.g., phosphorous and nitrate), and avoid harmful UV radiation while simultaneously harnessing beneficial regions of the visible electromagnetic spectrum via the selective attenuation of light (and selective avoidance of dissolved oxygen) within the water column.

Implications for planetary habitability and the search for life beyond Earth

The coevolution of environment and life early in Earth's history serves as a model for predicting universal, detectable biosignatures that might be generated on a microbe-dominated planet beyond our solar system. The current approach to constraining the possible suite of remotely detectable biosignatures leverages the aggregate spectral features of photosystems and pigment proteins which are sensitive to different portions of the Sun's emission spectrum (Fig. 5) (Schwieterman et al. 2018). Photosystems, representing an early-evolved phototrophic strategy (Oliver et al. 2021), exhibit an immense capacity for tunability that is intimately associated with the diverse properties of attached pigments (Cardona 2015; Nürnberg et al. 2018). However, they are complicated, specialized structures, as opposed to rhodopsins which are comparatively simple and consolidate a photosensitive mechanism into a single protein. The dual roles of rhodopsin active site residues as determinants of both function and peak photon absorptivity demonstrate that these pigment proteins generate a suite of biosignatures that are tunable to our Sun's peak irradiance profile, to long-term changes in the Earth surface chemical system, and to ecological niche diversification over billions of years. Our phylogenetic analysis indicates that rhodopsins' structural simplicity, functional variability and spectral tunability make them an ideal testbed for assessing universal properties of biosignature production on candidate microbe-dominated planets that may differ from our referent biological (Earth-Sun) system.

A generic characteristic of life is that it is 'tuned' to the conditions found on our planet that enable its existence. These conditions refer to the chemical and physical characteristics that circumscribe habitability, namely substrate availability, ambient temperature, pH, atmospheric pressure and composition, salt concentration, and solar insolation, and irradiance, among other geochemical and atmospheric attributes. As demonstrated here, proteins can be far more tuned to these external conditions than other molecules or anatomical features that compose organisms, precisely because many proteins serve as intermediaries for channelizing photons and substrates into metabolic activity. Our results show that protein families (and to some extent, the niches occupied by their hosts) can be amenable to paleobiological reconstruction in ways that cannot be accomplished using conventional molecular biosignatures alone.

Utilizing proteins as paleosensors of geologic and stellar conditions in deep time, leveraging the informatic characteristics of protein composition, and the tight coupling between internal (cellular) and external (environmental) conditions, permits future studies exploring circumstances of habitability and biosignature production over Earth's deep and varied history. Light absorbance profiles produced by microbial pigments can be used to prime future disk-

integrated observations of exoplanets, provide surficial albedo parameters for complex atmospheric radiative transfer models, and directly aid the development of instrumentation for the detection and characterization of life in the universe both within and outside our Solar System. Forthcoming integrative studies that reconcile experimentally validated biological photon absorbances with more sophisticated planetary system analyses would thus be beneficial, for instance, in applying microbial spectral properties to assess the potential habitability or inhabitation of extrasolar planets (Hegde 2015; Schwieterman 2015; DasSarma 2020). Overall, understanding biomolecular adaptations may benefit planetary habitability assessments when planetary and stellar indicators are poorly constrained.

METHODS

Phylogenetic reconstruction and ancestral sequence inference

A type 1 microbial rhodopsin protein sequence dataset was created by identifying homologs from the National Center for Biotechnology Information non-redundant protein database in December 2020. Homologous sequences were identified and obtained via BLASTp (Camacho et al. 2009) using query amino acid sequences acquired from UniProt (Uniprot Consortium 2019) (Supplementary Table 5) and an expect value cutoff of <1e-5. The sequence dataset was curated to remove duplicate and partial sequences. The final dataset consisted of 568 sequences: 96 bacteriorhodopsin, 144 halorhodopsin, 83 proteorhodopsin, 29 sensory rhodopsin I, 56 sensory rhodopsin II, 44 xanthorhodopsin, and 116 outgroup heliorhodopsin sequences. The dataset was aligned by MAFFT (v7.427) (Katoh and Standley 2013) with a gap open penalty of 1.53 and offset value of 0.0. Fungal and algal type 1 rhodopsin sequences were excluded from the dataset due to long-branch-attraction effects observed within the bacterial rhodopsin clade. In addition, viral rhodopsin sequences (Yutin and Koonin 2012) were excluded due to the paucity of relevant paleobiological indicators for tracking their evolution in the context of Earth surface environmental changes.

The rhodopsin protein sequence alignment was used to select the best-fit evolutionary model by ModelFinder (Kalyaanamoorthy et al. 2017) implemented in the W-IQ-TREE web server(Trifinopoulos et al. 2016). Models accounting for the proportion of invariant sites (“+I”) were not included in model selection due to issues optimizing rate heterogeneity parameters independently (Yang 2006). The three top-ranking models scored by the Akaike and Bayesian

Information Criterion, LG+G+F, WAG+G+F, and VT+G+F, were used for maximum likelihood phylogenetic inference by RAxML (v8) (Stamatakis 2014). Branch support was evaluated using 100 rapid bootstrap replicates. The type 1 rhodopsin clade was rooted with heliorhodopsin sequences, a protein group known to share a distant homology with type 1 rhodopsins (Pushkarev 2018; Shibukawa 2019). Because all tested evolutionary models yielded comparable topologies, the best-fit model, LG+G+F, was implemented for ancestral sequence inference by PAML (v4) (Yang 2007). Ancestral insertion/deletion sites were reconstructed using a binary likelihood model following Aadland et al. (2019).

Homology modeling and functional predictions of ancestral rhodopsin sequences

Inferred maximum likelihood ancestral sequences for the five deepest phylogenetic nodes (Anc1-Anc5) were submitted to the Phyre2 web server (Kelley et al. 2015) for structural homology modeling. Selected structural templates for modeling and associated statistics are listed in Supplementary Table 6. Predicted ancestral rhodopsin structures were used for structure-based functional annotation by COFACTOR implemented in the I-TASSER software suite (Roy 2010), which predicts protein function based on global and local similarities to template proteins with known structures and functions.

Alternative ancestral sequence library generation

For ancestral nodes Anc1-Anc5, 50 alternate protein sequences were generated from site-wise posterior probabilities to test the robustness of downstream analyses to statistical uncertainty of ancestral inference. For each ancestral node, regularly increasing percentages (>0% to 100%) of ambiguously reconstructed sites in the maximum likelihood sequence—defined here as having posterior probabilities <0.7—were replaced with the next most probable residue. Thus, the least probable ancestral sequence explored here by this approach had all ambiguous residues replaced by an alternate residue, likely representing the fringe of plausible ancestral sequence space (Eick et al. 2017).

Wavelength Prediction

Ancestral maximum absorbance wavelength (λ_{max}) values were predicted using the machine learning model, group-LASSO-based machine learning method (Karasuyama et al. 2018)

implemented in R. This statistical model describes the relationship between primary amino acid sequence and rhodopsin color tuning based on a training rhodopsin sequence dataset with experimentally validated λ_{max} values. Maximum likelihood and alternate ancestral rhodopsin sequences, as well as all extant rhodopsin sequences used for phylogenetic inference, were aligned to the training dataset for λ_{max} prediction.

Radiative transfer and pigment spectra

Surface photon irradiance spectra were calculated with the Spectral Mapping Atmospheric Radiative Transfer (SMART) model developed by D. Crisp (Meadows 1996). Calculation assumed cloud-free conditions with a solar zenith angle of 60 degrees and summed both direct and diffuse radiation at the surface. The modern Earth atmospheric profile was assumed to be a 1962 U.S. Standard Atmosphere employed by the InterComparison of Radiation Codes in Climate Models (ICRCCM) project (Luther 1988), whereas the Archean scenario was assumed to be a haze-free anoxic atmosphere from Arney et al. (2016) with a CH_4/CO_2 ratio of 0.1. The absorption coefficients of Segelstein (1981) and the Beer-Lambert Law were used to calculate the transmissivity and the attenuation of the photon irradiances as a function of depth.

Data availability

All code and phylogenetic datasets can be found at https://github.com/kacarlab/Rhodopsin.

ACKNOWLEDGEMENTS

We thank I. Takeuchi, M. Karasuyama, and K. Inoue for access to the machine learning algorithms used to predict rhodopsin wavelength absorbances used in this work, for the supportive assistance and the useful comments, and S. DasSarma for the insightful conversations. This work was supported by the NASA Arizona Space Grant (C.D.S.), the NASA Astrobiology Postdoctoral Fellowship, (A.K.G.), the NASA Interdisciplinary Astrobiology Research Consortium (ICAR) MUSE, a member of the NASA Early Cell to Multicellularity Research Coordination Network funded via the Astrobiology Research Program No 80NSSC21K0592 (B.K.), the NASA Early Career Faculty Award No. 80NSSC19K1617 (B.K.) and an NSF Emerging Frontiers Program Award No. 1724090 (B.K.), NASA's Alternative Earths team funded by the NASA Astrobiology Institute under Cooperative Agreement Number

NNA15BB03A and the NASA ICAR program, and the Virtual Planetary Laboratory, a member of the NASA Nexus for Exoplanet System Science (NExSS) funded via NASA Astrobiology Program Grant No. 80NSSC18K0829 (E.W.S.).

AUTHOR CONTRIBUTIONS

B.K. conceived and supervised the overall study. C.D.S. designed and performed the phylogenetic and modeling experiments, collected, and analyzed the data. E.F. designed and generated the ancient protein library and wavelength prediction pipeline with input from A.K.G. E.W.S. conducted the radiative transfer calculations and contributed to the habitability at depth hypothesis with input from Z.R.A. All authors discussed and interpreted the results. B.K. and C.D.S. wrote the manuscript with input and/or text contributions from all authors.

COMPETING INTERESTS STATEMENT

The authors declare no competing interests.

586 **REFERENCES**

587

588 Aadland K, Pugh C, Kolaczkowski B. 2019. High-Throughput Reconstruction of Ancestral
589 Protein Sequence, Structure, and Molecular Function. *Methods Mol Biol*. 1851:135-170. doi:
590 10.1007/978-1-4939-8736-8_8.

591 Adam ZR, Skidmore ML, Mogk DW, Butterfield NJ. 2017. A Laurentian record of the earliest
592 fossil eukaryotes. *Geology*. 45:387-390. doi: 10.1130/g38749.1.

593 Adam ZR, Skidmore, M.L., Mogk, D.M. 2016. Paleoenvironmental implications of an expanded
594 microfossil assemblage from the Chamberlain Formation, ower Belt Supergroup, Montanta. *The*
595 *Geological Society of America Special Paper*. 522.

596 Akram N, Palovaara, J., Forsberg, J., Lindh, M.V., Milton, D.L., Luo, H., González, J.M.,
597 Pinhassi, J. 2013. Regulation of proteorhodopsin gene expression by nutrient limitation in the
598 marine bacterium Vibrio sp. AND4. *Environmental microbiology*. 15:1400–1415. doi:
599 https://doi.org/10.1111/1462-2920.12085.

600 Arney G, Domagal-Goldman, S.D., Meadows, V.S., Wolf, E.T., Schwieterman, E., Charnay, B.,
601 Claire, M., Hébrard, E., Trainer, M.G. 2016. The Pale Orange Dot: The Spectrum and
602 Habitability of Hazy Arhean Earth. *Astrobiology*. 16:873-899. doi:
603 https://doi.org/10.1089/ast.2015.1422.

604 Babitzki G, Denschlag, R., Tavan, P. 2009. Polarization effects stabilize bacteriorhodopsin's
605 chromophore
606 binding pocket: a molecular dynamics study. *The journal of physical chemistry B*. 113:10483–
607 10495. doi: https://doi.org/10.1021/jp902428x.

608 Benner SA, Caraco, M.D., Thomson, J.M., Gaucher, E.A. 2002. Planetary biology—
609 paleontological, geological, and molecular histories of life. *Science*. 296:864-868. doi:
610 https://doi.org/10.1126/science.1069863.

611 Berhanu S, Ueda T, Kuruma Y. 2019. Artificial photosynthetic cell producing energy for protein
612 synthesis. *Nature Communications*. 10. doi: 10.1038/s41467-019-09147-4.

613 Besaw JE, Ou W-L, Morizumi T, Eger BT, Sanchez Vasquez JD, Chu JHY, Harris A, Brown LS,
614 Miller RJD, Ernst OP. 2020. The crystal structures of a chloride-pumping microbial rhodopsin

615 and its proton-pumping mutant illuminate proton transfer determinants. *J Biol Chem*. 295:14793-
616 14804. doi: 10.1074/jbc.RA120.014118.

617 Bogomolni RA, Stoeckenius W, Szundi I, Perozo E, Olson KD, Spudich JL. 1994. Removal of
618 transducer HtrI allows electrogenic proton translocation by sensory rhodopsin I. *Proc Natl Acad*
619 *Sci USA*. 91:10188-10192. doi: 10.1073/pnas.91.21.10188.

620 Bryant DA, Frigaard N-U. 2006. Prokaryotic photosynthesis and phototrophy illuminated. *Trends*
621 *in Microbiology*. 14:488-496. doi: 10.1016/j.tim.2006.09.001.

622 Burnetti A, Ratcliff W. 2020. The Origin of Phototrophy Reveals the Importance of Priority
623 Effects for Evolutionary Innovation. *Preprints*.2020110700.

624 Butterfield NJ. 2007. Macroevolution and Macroecology through Deep Time. *Palaeontology*.
625 50:41-55. doi: 10.1111/j.1475-4983.2006.00613.x.

626 Butterfield NJ, Rainbird RH. 1998. Diverse organic-walled fossils, including “possible
627 dinoflagellates,” from the early Neoproterozoic of arctic Canada. *Geology*. 26. doi:
628 10.1130/0091-7613(1998)026<0963:Dowfip>2.3.Co;2.

629 Camacho C, Coulouris G, Avagyan V, Ma N, Papadopoulos J, Bealer K, Madden TL. 2009.
630 BLAST+: architecture and applications. *BMC Bioinformatics*. 10:421. doi: 10.1186/1471-2105-
631 10-421.

632 Cardona T. 2018. Early Archean origin of heterodimeric Photosystem I. *Heliyon*. 4. doi:
633 10.1016/j.heliyon.2018.e00548.

634 Cardona T. 2015. A fresh look at the evolution and diversification of photochemical reaction
635 centers. *Photosynth Res*. 126:111-134. doi: 10.1007/s11120-014-0065-x.

636 Chazan A, Rozenberg A, Mannen K, Nagata T, Tahan R, Yaish S, Larom S, Inoue K, Beja O,
637 Pushkarev A. 2022. Diverse heliorhodopsins detected via functional metagenomics in
638 freshwater Actinobacteria, Chloroflexi and Archaea. *Environ Microbiol*. 24:110-121. doi:
639 10.1111/1462-2920.15890.

640 Chen M, Blankenship, R.E. 2011. Expanding the solar spectrum used by photosynthesis.
641 *Trends in Plant Science*. 16:427–431. doi: https://doi.org/10.1016/j.tplants.2011.03.011.

642 Chen M, Schliep, M., Willows, R.D., Cai, Z.-L., Neilan, B.A., Scheer, H. 2010. A Red-Shifted
643 Chlorophyll. *Science* 329:1318–1319. doi: https://doi.org/10.1126/science.1191127.

644 Damer B, Deamer, D. . 2020. The Hot Spring Hypothesis for an Origin of Life. *Astrobiology*.
645 20:429-452. doi: https://doi.org/10.1089/ast.2019.2045.

646 DasSarma P, Zamora RC, Muller JA, DasSarma S. 2012. Genome-wide responses of the
647 model archaeon Halobacterium sp. strain NRC-1 to oxygen limitation. *J Bacteriol*. 194:5530-
648 5537. doi: 10.1128/JB.01153-12.

649 DasSarma S, DasSarma, P., Laye, V.J., Schwieterman, E.W. 2020. Extremophilic models for
650 astrobiology: haloarchaeal survival strategies and pigments for remote sensing. *Extremophiles*
651 24:31–41. doi: https://doi.org/10.1007/s00792-019-01126-3.

652 DasSarma S, Schwieterman EW. 2018. Early evolution of purple retinal pigments on Earth and
653 implications for exoplanet biosignatures. *International Journal of Astrobiology*.1-10. doi:
654 10.1017/s1473550418000423.

655 Deamer DW, Dworkin JP. 2005. Chemistry and Physics of Primitive Membranes. In. Prebiotic
656 Chemistry. p. 1-27.

657 Ding X, Sun, C., Cui, H., Chen, S., Gao, Y., Yang, Y., Wang, J., He, X., Iuga, D., Tian, F., Watts,
658 A., Zhao, X. 2018. Functional roles of tyrosine 185 during the bacteriorhodopsin photocycle as
659 revealed by in situ spectroscopic studies. *Biochimica et biophysica acta: bioenergetics*.
660 1859:1006–1014. doi: https://doi.org/10.1016/j.bbabio.2018.05.011.

661 Doolittle WF. 2000. The nature of the universal ancestor and the evolution of the proteome.
662 *Current opinion in structural biology*. 10:355–358. doi: https://doi.org/10.1016/s0959-
663 440x(00)00096-8.

664 Eick GN, Bridgham JT, Anderson DP, Harms MJ, Thornton JW. 2017. Robustness of
665 Reconstructed Ancestral Protein Functions to Statistical Uncertainty. *Mol Biol Evol*. 34:247-261.
666 doi: 10.1093/molbev/msw223.

667 Engelhard C, Chizhov I, Siebert F, Engelhard M. 2018. Microbial Halorhodopsins: Light-Driven
668 Chloride Pumps. *Chemical Reviews*. 118:10629-10645. doi: 10.1021/acs.chemrev.7b00715.

669 Engqvist MKM, McIsaac RS, Dollinger P, Flytzanis NC, Abrams M, Schor S, Arnold FH. 2015.
670 Directed Evolution of Gloeobacter violaceus Rhodopsin Spectral Properties. *Journal of*
671 *Molecular Biology*. 427:205-220. doi: https://doi.org/10.1016/j.jmb.2014.06.015.

672 Ernst OP, Lodowski, D.T., Elstner, M., Hegemann, P., Brown, L.S., Kandori, H. 2014. Microbial
673 and Animal Rhodopsins: Structures, Functions, and Molecular Mechanisms. *Chemical Reviews*.
674 114:126–163. doi: https://doi.org/10.1021/cr4003769.

675 Finkel OM, Béjà O, Belkin S. 2012. Global abundance of microbial rhodopsins. *The ISME*
676 *Journal*. 7:448-451. doi: 10.1038/ismej.2012.112.

677 Frigaard N, Larsen, Kim, L., Cox, R.P. 1996. Spectrochromatography of photosynthetic
678 pigments as a fingerprinting technique for microbial phototrophs. *FEMS Microbiology Ecology*.
679 20:69–77. doi: https://doi.org/10.1016/0168-6496(96)00005-0.

680 Garcia AK, Cavanaugh CM, Kacar B. 2021. The curious consistency of carbon biosignatures
681 over billions of years of Earth-life coevolution. *ISME J*. doi: 10.1038/s41396-021-00971-5.

682 Garcia AK, Kaçar, B. 2019. How to resurrect ancestral proteins as proxies for ancient
683 biogeochemistry. *Free Radical Biology and Medicine*. 140:260-269. doi:
684 https://doi.org/10.1016/j.freeradbiomed.2019.03.033.

685 Gómez-Conarnau L, Raven, J.A., Levine, N.M., Cutter, L.S., Wang, D., Seegers, B., Arístegui,
686 J., Fuhrman, J.A., Gasol, J.M., Sañudo-Wilhelmy, S.A. . 2019. Microbial rhodopsins are major
687 contributors to the solar energy captured in the sea. *Science Advances*. 5:eaaw8855. doi:
688 https://doi.org/10.1126/sciadv.aaw8855.

689 Govorunova E, Sineshchekov, O.A., Li, H., Spudich, J.L. 2017. Microbial Rhodopsins: Diversity,
690 Mechanisms, and Optogenetic Applications. *Annual Review of Biochemistry*. 86:845-872. doi:
691 https://doi.org/10.1146/annurev-biochem-101910-144233.

692 Greenhalgh DA, Farrens, D.L., Subramaniam, S., Khorana, H.G. 1993. Hydrophobic Amino
693 Acids in the Retinal-binding Pocket of Bacteriorhodopsin. *The Journal of Biological Chemistry*.
694 268:20305-20311. doi: https://doi.org/10.1016/S0021-9258(20)80729-7.

695 Hampp N, Oesterhelt D. 2004. Bacteriorhodopsin and Its Potential in Technical Applications. In:
696 Niemeyer CM, Mirkin CA, editors. Nanobiotechnology. p. 146-167.

Harrison JP, Gheeraert, N., Tsigelnitskiy, D., Cockell, C.S. 2013. The limits for life under multiple extremes. *Trends in microbiology*. 21:204-212. doi: https://doi.org/10.1016/j.tim.2013.01.006.

Hasegawa M, Hosaka T, Kojima K, Nishimura Y, Nakajima Y, Kimura-Someya T, Shirouzu M, Sudo Y, Yoshizawa S. 2020. A unique clade of light-driven proton-pumping rhodopsins evolved in the cyanobacterial lineage. *Sci Rep*. 10:16752. doi: 10.1038/s41598-020-73606-y.

Hazen RM, Golden J, Downs RT, Hystad G, Grew ES, Azzolini D, Sverjensky DA. 2012. Mercury (Hg) mineral evolution: A mineralogical record of supercontinent assembly, changing ocean geochemistry, and the emerging terrestrial biosphere. *American Mineralogist*. 97:1013-1042. doi: 10.2138/am.2012.3922.

Hegde S, Paulino-Lima, I.G., Kent, R., Kaltenegger, L., Rothschild, L. 2015. Surface biosignatures of exo-Earths: Remote detection of extraterrestrial life. *Proceedings of the National Academy of Sciences*. 112:3886–3891. doi: https://doi.org/10.1073/pnas.1421237112.

Hirokawa T, Boon-Chieng S, Mitaku S. 1998. SOSUI: classification and secondary structure prediction system for membrane proteins. *Bioinformatics*. 14:378-379. doi: 10.1093/bioinformatics/14.4.378.

Hofmann HJ, Jackson GD. 1994. Shale-Facies Microfossils from the Proterozoic Bylot Supergroup, Baffin Island, Canada. *J Paleontol*. 68:1-35. doi: 10.1017/s0022336000062314.

Ihara K, Umemura, T., Katagiri, I., Kitajima-Ihara, T., Sugiyama, Y., Kimura, Y., & Mukohata, Y. 1999. Evolution of the archaeal rhodopsins: evolution rate changes by gene duplication and functional differentiation. *Journal of molecular biology*. 285:163–174. doi: https://doi.org/10.1006/jmbi.1998.2286.

Inoue K. 2020. Shining light on rhodopsin selectivity: How do proteins decide whether to transport H+ or Cl–? *J Biol Chem*. 295:14805-14806. doi: 10.1074/jbc.H120.016032.

Inoue K, Karasuyama, M., Nakamura, R., Konno, M., Yamada, D., Mannen, K., Nagata, T., Inatsu, Y., Yawo, H., Yura, K., Béjà, O., Kandori, H., Takeuchi, I. . 2021. Exploration of natural red-shifted rhodopsins using a machine learning-based Bayesian experimental design. *Communications biology*. 4:362. doi: https://doi.org/10.1038/s42003-021-01878-9.

725 Inoue K, Tahara S, Kato Y, Takeuchi S, Tahara T, Kandori H. 2018. Spectroscopic Study of
726 Proton-Transfer Mechanism of Inward Proton-Pump Rhodopsin, Parvularcula oceani
727 Xenorhodopsin. *The Journal of Physical Chemistry B*. 122:6453-6461. doi:
728 https://doi.org/10.1021/acs.jpcb.8b01279.

729 Javaux EJ, Knoll, A.H. 2017. Micropaleontology of the lower Mesoproterozoic Roper Group,
730 Australia, and implications for early eukaryotic evolution. *Journal of Paleontology*. 91:199-229.
731 doi: https://doi.org/10.1017/jpa.2016.124.

732 Jeffrey SW. 1963. Purification and properties of chlorophyll c from Sargassum flavicans.
733 *Biochemical Journal*. 86:313-318. doi: https://doi.org/10.1042/bj0860313.

734 Kacar B, Guy L, Smith E, Baross J. 2017. Resurrecting ancestral genes in bacteria to interpret
735 ancient biosignatures. *Philos Trans R Soc A*. 375. doi: 10.1098/rsta.2016.0352.

736 Kalyaanamoorthy S, Minh BQ, Wong TKF, von Haeseler A, Jermiin LS. 2017. ModelFinder: fast
737 model selection for accurate phylogenetic estimates. *Nature Methods*. 14:587-589. doi:
738 10.1038/nmeth.4285.

739 Kandori H. 2015. Ion-pumping microbial rhodopsins. *Front Mol Biosci*. 2:52. doi:
740 10.3389/fmolb.2015.00052.

741 Karasuyama M, Inoue K, Nakamura R, Kandori H, Takeuchi I. 2018. Understanding Colour
742 Tuning Rules and Predicting Absorption Wavelengths of Microbial Rhodopsins by Data-Driven
743 Machine-Learning Approach. *Sci Rep*. 8:15580. doi: 10.1038/s41598-018-33984-w.

744 Katoh K, Standley DM. 2013. MAFFT multiple sequence alignment software version 7:
745 improvements in performance and usability. *Mol Biol Evol*. 30:772-780. doi:
746 10.1093/molbev/mst010.

747 Kelley LA, Mezulis S, Yates CM, Wass MN, Sternberg MJE. 2015. The Phyre2 web portal for
748 protein modeling, prediction and analysis. *Nature Protocols*. 10:845-858. doi:
749 10.1038/nprot.2015.053.

750 Kusnetzow A, Singh, D.L., Martin, C.H., Barani, I.J., Birge, R.R. 1999. Nature of the
751 chromophore binding site of bacteriorhodopsin: the potential role of Arg82 as a principal

counterion. *Biophysical journal*. 76:2370–2389. doi: https://doi.org/10.1016/S0006-3495(99)77394-7.

Lamsdell JC, Congreve CR, Hopkins MJ, Krug AZ, Patzkowsky ME. 2017. Phylogenetic Paleoecology: Tree-Thinking and Ecology in Deep Time. *Trends in Ecology & Evolution*. 32:452-463. doi: 10.1016/j.tree.2017.03.002.

Lane N, Allen JF, Martin W. 2010. How did LUCA make a living? Chemiosmosis in the origin of life. *Bioessays*. 32:271-280. doi: 10.1002/bies.200900131.

Lu Y, Zhou XE, Gao X, Wang N, Xia R, Xu Z, Leng Y, Shi Y, Wang G, Melcher K, et al. 2019. Crystal structure of heliorhodopsin 48C12. *Cell Research*. 30:88-90. doi: 10.1038/s41422-019-0266-0.

Lunine JI. 2006. Physical conditions on the early Earth. *Philosophical Transactions of the Royal Society B*. 361:1721-1731. doi: https://doi.org/10.1098/rstb.2006.1900.

Luther FM, Ellingson, R.G., Fouquart, Y., Fels, S., Scott, N.A., Wiscombe, W.J. 1988. Intercomparison of Radiation Codes in Climate Models (ICRCCM): Longwave Clear-Sky Results—A Workshop Summary. *Bulletin of the American Meteorological Society*. 69:40-48. doi: https://doi.org/10.1175/1520-0477-69.1.40.

Lyons TW, Reinhard CT, Planavsky NJ. 2014. The rise of oxygen in Earth's early ocean and atmosphere. *Nature*. 506:307-315. doi: 10.1038/nature13068.

Mackin KA, Roy, R.A., Theobald, D.L. 2014. An empirical test of convergent evolution in rhodopsins. *Molecular biology and evolution*. 31:85–95. doi: https://doi.org/10.1093/molbev/mst171.

Maloney PC, Wilson, T.H. 1985. The Evolution of Ion Pumps. *BioScience*. 35:43-48. doi: https://doi.org/10.2307/1310083.

Man D. 2003. Diversification and spectral tuning in marine proteorhodopsins. *EMBO J*. 22:1725-1731. doi: 10.1093/emboj/cdg183.

Mascarenhas V, Keck T. 2018. Marine Optics and Ocean Color Remote Sensing. In. YOUMARES 8 – Oceans Across Boundaries: Learning from each other. p. 41-54.

McKay CP. 2014. Requirements and limits for life in the context of exoplanets. *Proceedings of the National Academy of Sciences*. 111:12628-12633. doi: https://doi.org/10.1073/pnas.1304212111.

Meadows VS, Crisp, D. 1996. Ground-based near-infrared observations of the Venus nightside: The thermal structure and water abundance near the surface. *Journal of Geophysical Research: Planets*. 101:4595-4622. doi: https://doi.org/10.1029/95JE03567.

Mulkidjanian AY, Galperin MY, Koonin EV. 2009. Co-evolution of primordial membranes and membrane proteins. *Trends Biochem Sci*. 34:206-215. doi: 10.1016/j.tibs.2009.01.005.

Nakajima Y, Kojima K, Kashiyama Y, Doi S, Nakai R, Sudo Y, Kogure K, Yoshizawa S. 2020. Bacterium Lacking a Known Gene for Retinal Biosynthesis Constructs Functional Rhodopsins. *Microbes Environ*. 35. doi: 10.1264/jsme2.ME20085.

Newman MJ, Rood, R.T. 1977. Implications of Solar Evolution for the Earth's Early Atmosphere. *Science*. 198:1035-1037. doi: https://doi.org/10.1126/science.198.4321.1035.

Nürnberg DJ, Morton J, Santabarbara S, Telfer A, Joliot P, Antonaru LA, Ruban AV, Cardona T, Krausz E, Boussac A, et al. 2018. Photochemistry beyond the red limit in chlorophyll f–containing photosystems. *Science*. 360:1210-1213. doi: 10.1126/science.aar8313.

Oliver T, Sanchez-Baracaldo P, Larkum AW, Rutherford AW, Cardona T. 2021. Time-resolved comparative molecular evolution of oxygenic photosynthesis. *Biochim Biophys Acta Bioenerg*. 1862:148400. doi: 10.1016/j.bbabio.2021.148400.

Olson SL, Kump LR, Kasting JF. 2013. Quantifying the areal extent and dissolved oxygen concentrations of Archean oxygen oases. *Chem Geol*. 362:35-43. doi: 10.1016/j.chemgeo.2013.08.012.

Ozaki Y, Kawashima T, Abe-Yoshizumi R, Kandori H. 2014. A color-determining amino acid residue of proteorhodopsin. *Biochemistry*. 53:6032-6040. doi: 10.1021/bi500842w.

Penny D, Sojo V, Pomiankowski A, Lane N. 2014. A Bioenergetic Basis for Membrane Divergence in Archaea and Bacteria. *PLoS Biology*. 12. doi: 10.1371/journal.pbio.1001926.

805 Pinhassi J, DeLong, E.F., Béjà, O., González, J.M., Pedrós-Alió, C. 2016. Marine Bacterial and
806 Archaeal Ion-Pumping Rhodopsins: Genetic Diversity, Physiology, and Ecology. *Microbiology*
807 *and Molecular Biology Reviews*. 80:929–954. doi: https://doi.org/10.1128/MMBR.00003-16.

808 Pohorille A, Deamer, D. . 2009. Self-assembly and function of primitive cell membranes.
809 *Research in Microbiology*. 160:449-456. doi: https://doi.org/10.1016/j.resmic.2009.06.004.

810 Pohorille A, Wilson MA, Chipot C. 2003. *Origins of Life and Evolution of the Biosphere*. 33:173-
811 197. doi: 10.1023/a:1024627726231.

812 Pushkarev A, Inoue, K., Larom, S., Flores-Uribe, J., Singh, M., Konno, M., Tomida, S., Ito, S.,
813 Nakamura, R., Tsunoda, S. P., Philosof, A., Sharon, I., Yutin, N., Koonin, E. V., Kandori, H.,
814 Béjà, O. . 2018. A distinct abundant group of microbial rhodopsins discovered using functional
815 metagenomics. *Nature*. 558:595–599. doi: https://doi.org/10.1038/s41586-018-0225-9.

816 Racker E, Stoeckenius, W. 1974. Reconstitution of purple membrane vesicles catalyzing light-
817 driven proton uptake and adenosine triphosphate formation. *The Journal of Biological*
818 *Chemistry*. 249:662–663. doi: https://doi.org/10.1016/S0021-9258(19)43080-9.

819 Ren L, Martin CH, Wise KJ, Gillespie NB, Luecke H, Lanyi JK, Spudich JL, Birge RR. 2001.
820 Molecular Mechanism of Spectral Tuning in Sensory Rhodopsin II. *Biochemistry*. 40:13906-
821 13914. doi: 10.1021/bi0116487.

822 Roy A, Kucukural, A., Zhang, Y. 2010. I-TASSER: a unified platform for automated protein
823 structure and function prediction. *Nature Protocols*. 5:725–738. doi:
824 https://doi.org/10.1038/nprot.2010.5.

825 Rozenberg A, Inoue K, Kandori H, Béjà O. 2021. Microbial Rhodopsins: The Last Two Decades.
826 *Annual Review of Microbiology*. 75:427-447. doi: 10.1146/annurev-micro-031721-020452.

827 Ruiz-Gonzalez MX, Marin I. 2004. New insights into the evolutionary history of type 1
828 rhodopsins. *J Mol Evol*. 58:348-358. doi: 10.1007/s00239-003-2557-8.

829 Sánchez-Baracaldo P, Bianchini G, Wilson JD, Knoll AH. 2021. Cyanobacteria and
830 biogeochemical cycles through Earth history. *Trends in Microbiology*. doi:
831 10.1016/j.tim.2021.05.008.

Sasaki J, Brown LS, Chon Y-S, Kandori H, Maeda A, Needleman R, Lanyi JK. 1995. Conversion of Bacteriorhodopsin into a Chloride Ion Pump. *Science*. 269:73-75. doi: 10.1126/science.7604281.

Schwieterman EW, Cockell, C.S., Meadows, V.S. 2015. Nonphotosynthetic Pigments as Potential Biosignatures. *Astrobiology* 15:341–361. doi: https://doi.org/10.1089/ast.2014.1178.

Schwieterman EW, Kiang NY, Parenteau MN, Harman CE, DasSarma S, Fisher TM, Arney GN, Hartnett HE, Reinhard CT, Olson SL, et al. 2018. Exoplanet Biosignatures: A Review of Remotely Detectable Signs of Life. *Astrobiology*. 18:663-708. doi: https://doi.org/10.1089/ast.2017.1729.

Segelstein DJ. 1981. The complex refractive index of water. *University of Missouri*. doi: http://hdl.handle.net/10355/11599.

Shalaeva DN, Galperin, M.Y., Mulkidjanian, A.Y. 2015. Eukaryotic G protein-coupled receptors as descendants of prokaryotic sodium-translocating rhodopsins. *Biology Direct*. 10:1-12. doi: https://doi.org/10.1186/s13062-015-0091-4.

Sharma AK. 2009. Insights into the ecology and evolution of the light-harvesting microbial rhodopsins. [Dalhousie University.

Sharma AK, Spudich, J. L., Doolittle, W.F. 2006. Microbial rhodopsins: functional versatility and genetic mobility. *Trends in microbiology*. 14:463–469. doi: https://doi.org/10.1016/j.tim.2006.09.006.

Sharma AK, Walsh, D.A., Bapteste, E., Rodriguez-Valera, F., Ford Doolittle, W., Papke, R.T. 2007. Evolution of rhodopsin ion pumps in haloarchaea. *BMC evolutionary biology*. 7:1-13. doi: https://doi.org/10.1186/1471-2148-7-79.

Shibata M, Inoue, K., Ikeda, K., Konno, M., Singh, M., Kataoka, C., Abe-Yoshizumi, R., Kandori, H., & Uchihashi, T. . 2018. Oligomeric states of microbial rhodopsins determined by high-speed atomic force microscopy and circular dichroic spectroscopy. *Scientific reports*. 8:8262. doi: https://doi.org/10.1038/s41598-018-26606-y.

Shibukawa A, Kojima, K., Nakajima, Y., Nishimura, Y., Yoshizawa, S., Sudo, Y. . 2019. Photochemical Characterization of a New Heliorhodopsin from the Gram-Negative Eubacterium

Bellilinea caldifistulae (BcHeR) and Comparison with Heliorhodopsin-48C12. *Biochemistry*. 58:2934–2943. doi: https://doi.org/10.1021/acs.biochem.9b00257.

Song Y, Gunner MR. 2014. Halorhodopsin pumps Cl- and bacteriorhodopsin pumps protons by a common mechanism that uses conserved electrostatic interactions. *Proc Natl Acad Sci USA*. 111:16377-16382. doi: 10.1073/pnas.1411119111.

Spudich JL, Bogomolni RA. 1984. Mechanism of colour discrimination by a bacterial sensory rhodopsin. *Nature*. 312:509-513. doi: 10.1038/312509a0.

Stamatakis A. 2014. RAxML version 8: a tool for phylogenetic analysis and post-analysis of large phylogenies. *Bioinformatics*. 30:1312-1313. doi: 10.1093/bioinformatics/btu033.

Steindler L, Schwalbach, M.S., Smith, D.P., Chan, F., Giovannoni, S.J. . 2011. Energy starved *Candidatus* Pelagibacter ubique substitutes light-mediated ATP production for endogenous carbon respiration. *PloS one*. 6:e19725. doi: https://doi.org/10.1371/journal.pone.0019725.

Sudo Y, Furutani Y, Kandori H, Spudich JL. 2006. Functional importance of the interhelical hydrogen bond between Thr204 and Tyr174 of sensory rhodopsin II and its alteration during the signaling process. *J Biol Chem*. 281:34239-34245. doi: 10.1074/jbc.M605907200.

Trifinopoulos J, Nguyen L-T, von Haeseler A, Minh BQ. 2016. W-IQ-TREE: a fast online phylogenetic tool for maximum likelihood analysis. *Nucleic Acids Research*. 44:W232-W235. doi: 10.1093/nar/gkw256.

Tsujimura M, Ishikita H. 2020. Insights into the Protein Functions and Absorption Wavelengths of Microbial Rhodopsins. *The Journal of Physical Chemistry B*. 124:11819-11826. doi: 10.1021/acs.jpcb.0c08910.

Ueda H, Shibuya, T. 2021. Composition of the primordial ocean just after its formation: Constraints from the reactions between the primitive crust and a strongly acidic, CO2-rich fluid at elevated temperatures and pressures. *Minerals*. 11. doi: https://doi.org/10.3390/min11040389.

Ugalde JA, Podell S, Narasingarao P, Allen EE. 2011. Xenorhodopsins, an enigmatic new class of microbial rhodopsins horizontally transferred between archaea and bacteria. *Biology Direct*. 6. doi: 10.1186/1745-6150-6-52.

888 Uniprot Consortium. 2019. UniProt: a worldwide hub of protein knowledge. *Nucleic Acids*
889 *Research*. 47:D506-D515. doi: 10.1093/nar/gky1049.

890 Wilde A, Mullineaux CW. 2017. Light-controlled motility in prokaryotes and the problem of
891 directional light perception. *FEMS Microbiology Reviews*. 41:900-922. doi:
892 10.1093/femsre/fux045.

893 Yang Z. 2006. Computational Molecular Evolution. Oxford: Oxford University Press.

894 Yang Z. 2007. PAML 4: Phylogenetic Analysis by Maximum Likelihood. *Molecular Biology and*
895 *Evolution*. 24:1586–1591. doi: https://doi.org/10.1093/molbev/msm088.

896 Yutin N, Koonin EV. 2012. Proteorhodopsin genes in giant viruses. *Biology Direct*. 7. doi:
897 10.1186/1745-6150-7-34.
898
899

900 **FIGURES**

901

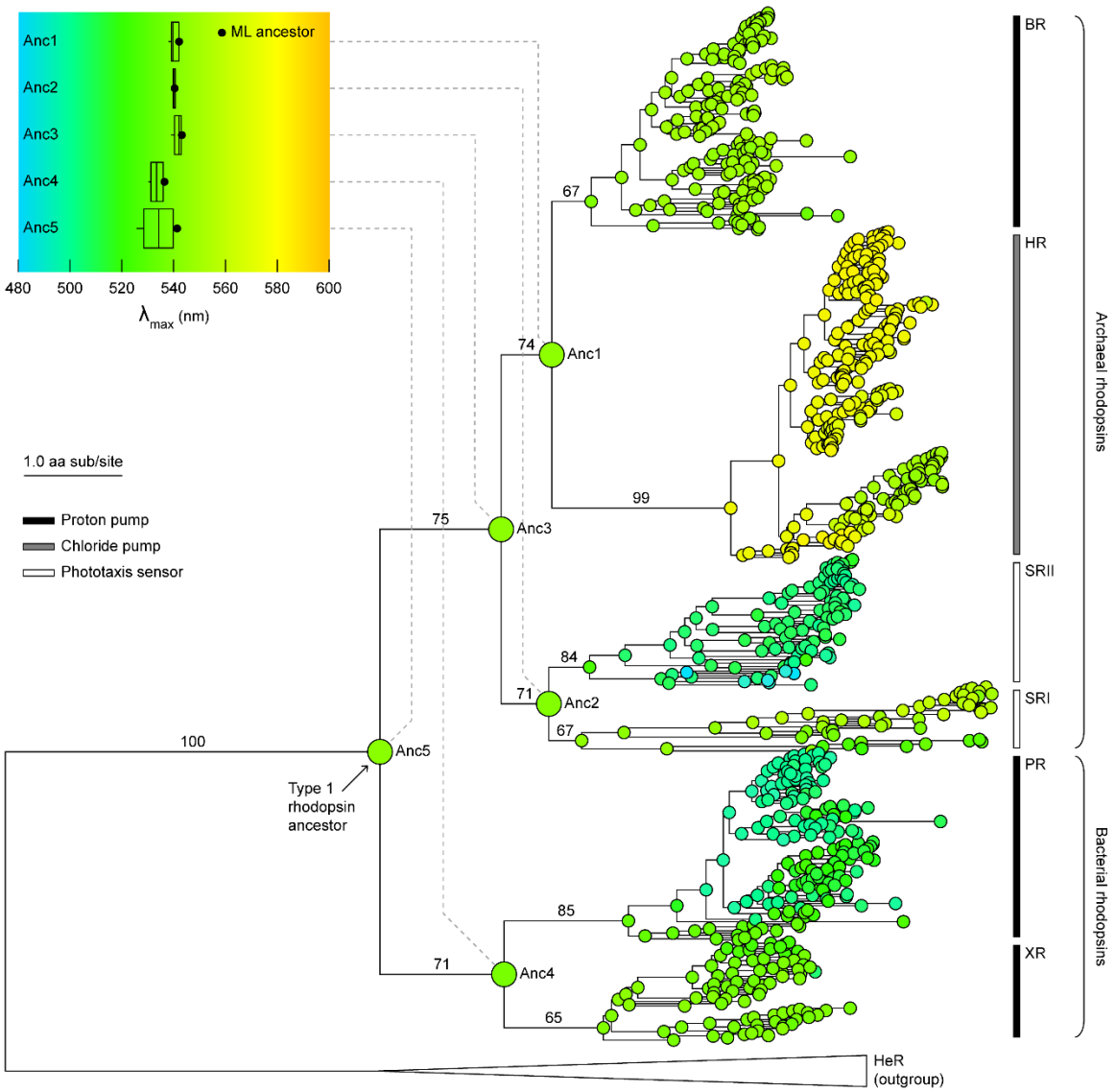

902

903 **Fig. 1. Evolution of spectral tuning mapped to a maximum likelihood phylogeny of**
904 **microbial type 1 rhodopsin protein sequences.** Nodes are colored according to the predicted
905 maximum absorption wavelength (λ_{max}) of the associated maximum likelihood (ML) ancestral
906 sequence (color scale shown in plot, top left). Boxplot shows the predicted λ_{max} distribution
907 among alternate ancestral sequences for nodes Anc1-Anc5 (n = 50 per node; see Methods and
908 Fig. 2b,c). Branch support values are derived from 100 bootstrap replicates. Branch scale
909 indicates 1.0 amino acid substitutions per site. Heliorhodopsin outgroup clade is collapsed. BR:
910 bacteriorhodopsin; HR, halorhodopsin; SR II, sensory rhodopsin II; SR I, sensory rhodopsin
911 I; PR, proteorhodopsin; XR, xanthorhodopsin; HeR, heliorhodopsin.

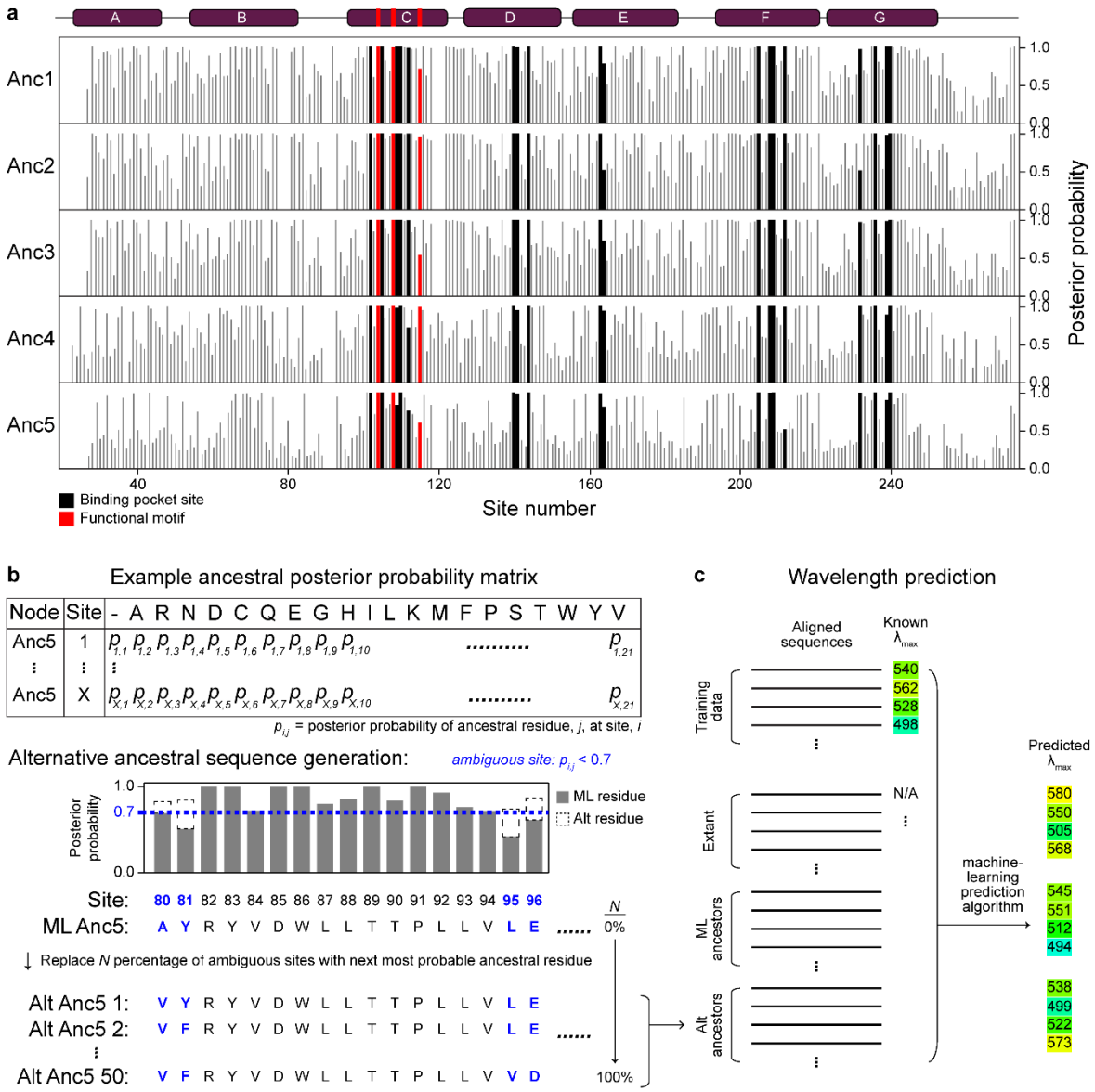

913

914 **Fig. 2. Incorporation of statistical uncertainty of ancestral rhodopsins inference into**
915 **wavelength prediction.** (*A*) Site-wise posterior probabilities of maximum likelihood (ML)
916 ancestral rhodopsin sequences. Sites labeled "functional motif" are homologous to the three-
917 residue DTD motif in extant *H. salinarum* bacteriorhodopsin. Helices are labeled above. (*B*)
918 Generation of alternative ("alt") ancestral sequences. For each node, alternate sequences were
919 generated by replacing 0% to 100% of ambiguous sites (defined as having a posterior
920 probability < 0.7) with the next most probable residue. (*C*) Methodology for maximum
921 absorbance wavelength (λ_{max}) prediction. λ_{max} values of extant and ancestral (both ML and
922 alternative) rhodopsin sequences were predicted by a machine-learning model (group-LASSO-

923 based machine learning method), trained on a dataset of experimentally characterized
924 rhodopsin proteins with known λ_{max} values.
925

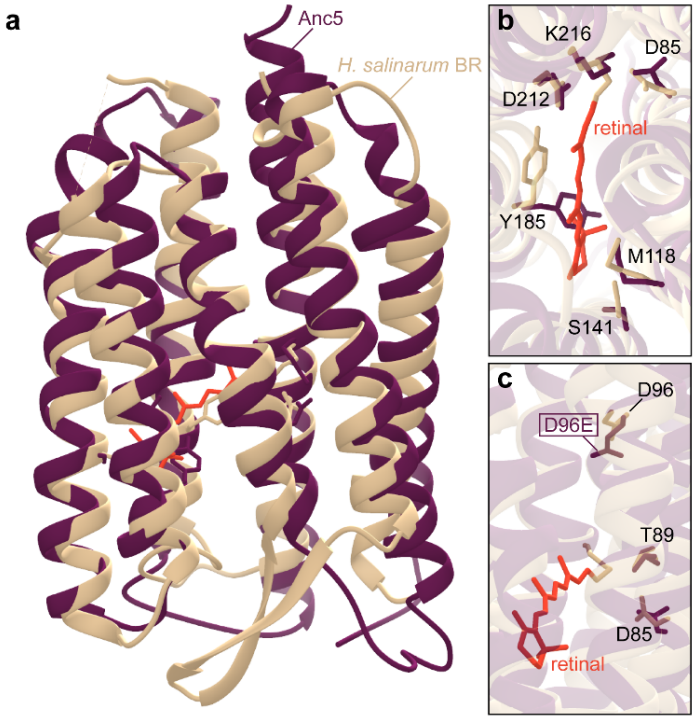

926
927 **Fig. 3. Structural conservation between the inferred, type 1 rhodopsin last common**
928 **ancestor, Anc5, and extant bacteriorhodopsin**. (*A*) Homology model of Anc5 aligned to the
929 extant *H. salinarum* bacteriorhodopsin ("BR"; PDB: 1C3W). (*B*) Retinal binding pocket of
930 ancestral and extant rhodopsins. Conserved residues that interact with the retinal chromophore
931 are labeled. (*C*) Residues homologous to the *H. salinarum* DTD motif correlative with rhodopsin
932 function. Extant bacteriorhodopsin exhibits a DTD motif, compared to the DTE motif in Anc5.
933 (*B*,*C*) All displayed Anc5 residues are identical to those of extant bacteriorhodopsin except for
934 site 96 (D96E, boxed).
935
936

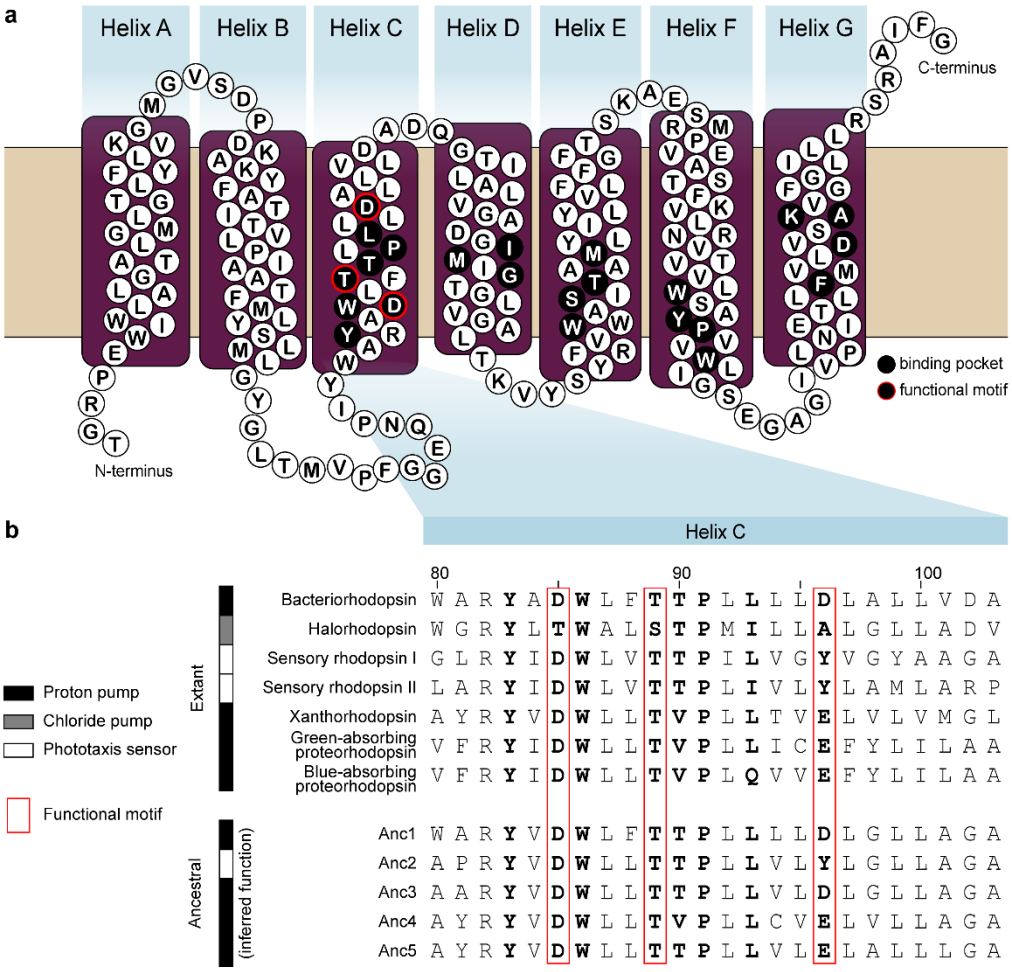

Fig. 4. Rhodopsin binding pocket residues in extant and inferred ancestral sequences. (*A*) Secondary structure of extant *H. salinarum* bacteriorhodopsin, indicating the binding pocket residues as well as the functionally correlative DTD motif. (*B*) Protein sequence alignment of Helix C residues for representative, extant type 1 rhodopsins and ancestral rhodopsins. Binding pocket residues are indicated by bold font. (*A*,*B*) Sites labeled "functional motif" are homologous to the three-residue DTD motif in extant *H. salinarum* bacteriorhodopsin.

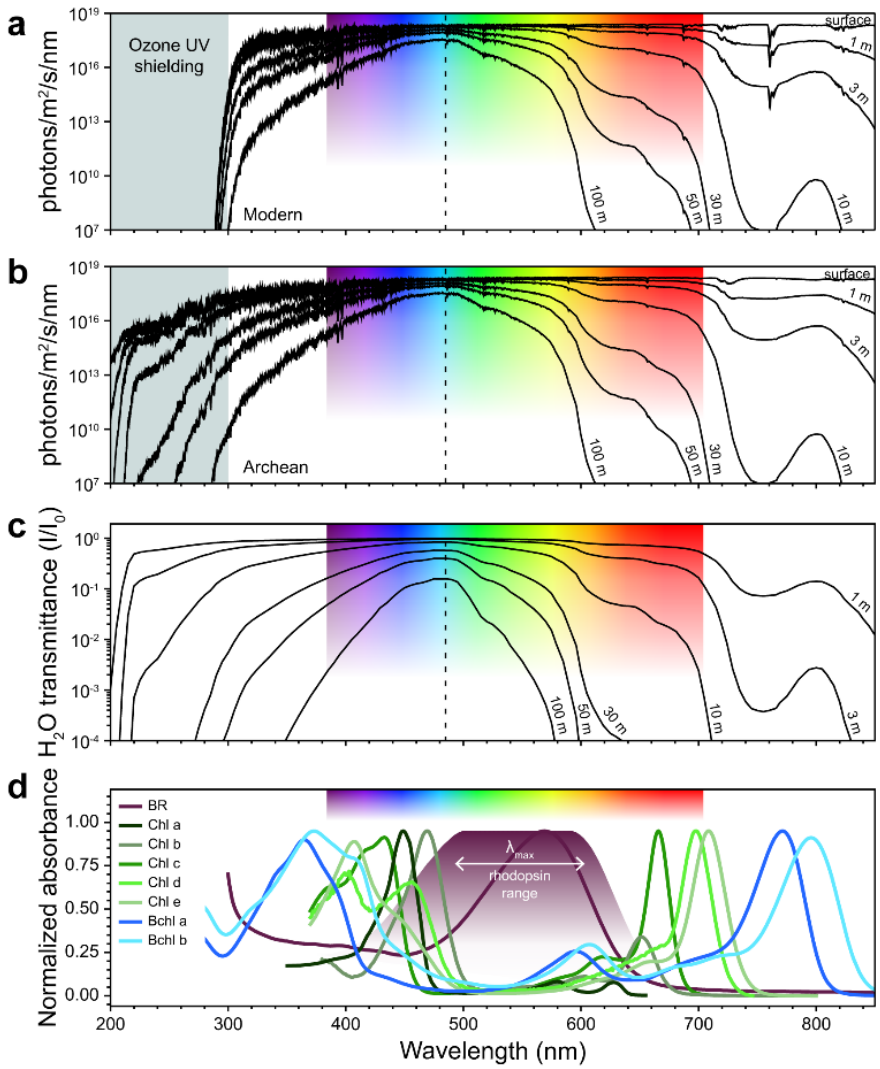

Fig. 5. Diversity of biological pigment absorbance profiles in the context of changing surface photon irradiance over Earth history. (*A*,*B*) Photon irradiance profiles at varying water depths, given a modern (*A*) or Archean (*B*) atmospheric composition. (*C*) Water transmission profile at varying water depths. Transmission was calculated from the coefficients of Segelstein (1981) and the Beer-Lambert Law. (*A*,*B*,*C*) Vertical dashed line indicates the maximum water transmission wavelength of 485 nm. (*D*) Normalized absorbance for bacteriorhodopsin ("BR"), chlorophylls ("Chl"), and bacteriochlorophylls ("Bchl"). Shaded purple region indicates the extant and ancestral range of predicted rhodopsin absorption peaks in Fig. 1. Chlorophyll and bacteriochlorophyll spectra are sourced from the Virtual Planetary Laboratory's Biological Pigments Database (http://vplapps.astro.washington.edu/pigments), with contributions from Jeffrey (1963), Frigaard (1996), and Chen (2010, 2011). The bacteriohodopsin spectrum was sourced from DasSarma and Schwieterman (2018).

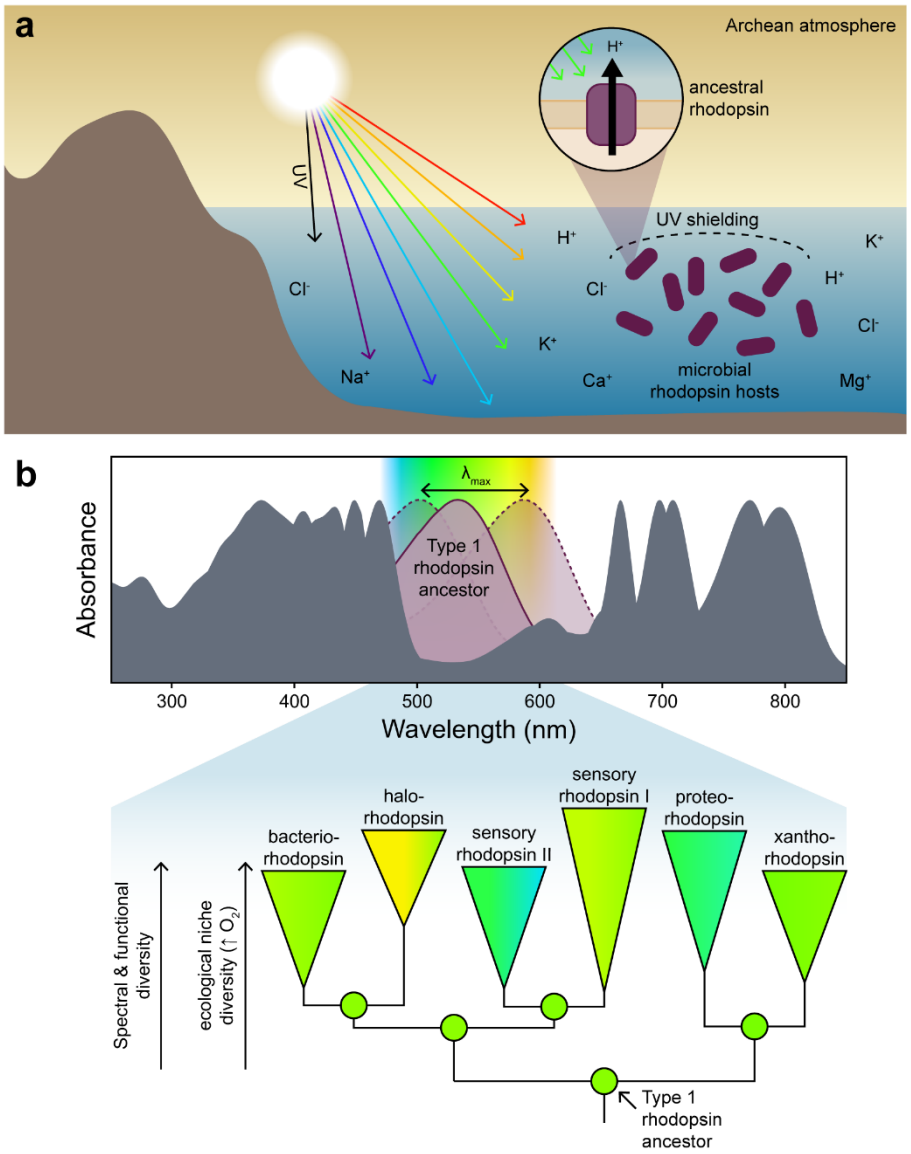

959

960 **Fig. 6. Coupling between surface irradiance, spectral tuning, and functional diversity**
961 **over microbial rhodopsin evolution.** (*A*) In a possible evolutionary scenario, microbial hosts
962 of ancestral type 1 rhodopsins could have occupied depths in the Archean marine environment
963 where high UV irradiation was attenuated and where they could have absorbed green
964 wavelengths to which they were maximally tuned. These ancestral rhodopsins would likely have
965 functioned as light-driven proton pumps, providing both a simplistic means of energy production
966 and maintenance of the intracellular environment. (*B*) Color tuning of extant and ancestral
967 microbial rhodopsins appear to explore the spectral window not already occupied by other
968 biological pigments such as chlorophylls and bacteriochlorophylls (grey, adapted from Fig. 5d).
969 Spectral diversification over rhodopsin evolutionary history likely accompanied functional

970 specialization enabled by the expanded ecological niches following the rise of atmospheric
971 oxygen.